Full Text View

Volume 30, Issue 2 (February 2000)

Journal of Physical Oceanography
Article: pp. 369–384 | Abstract | PDF (950K)

A Numerical Study on the Coastal Topographic Effect of a Peninsula on the Western Boundary Current

Yoshihiko Sekine

Institute of Oceanography, Faculty of Bioresources, Mie University, Tsu, Japan

(Manuscript received January 2, 1997, in final form April 5, 1999)

DOI: 10.1175/1520-0485(2000)030<0369:ANSOTC>2.0.CO;2

ABSTRACT

Coastal topographic effects of a peninsula on the western boundary current are studied numerically with reference to the difference in northern boundary inclination (NBI) from a zonal direction. It is shown from the numerical experiments that the two dominant path patterns of the western boundary current exist: one flow pattern is a large meander path with spinup and spindown of the cyclonic eddy and the other is a nonlarge (straight) path along the northern boundary. If a peninsula is located upstream (west) of the separation point of the mean flow flowing out from the northernmost area of the western boundary region, a large meander path with spinup and spindown of the cyclonic eddy is changed to an irregular oscillation by the topographic effect of the peninsula in the case of no NBI. A nonlarge meander path with a small cyclonic eddy just downstream of the peninsula is formed in the cases with NBI larger than 10°. Formation of the large meander path and the nonlarge meander path agrees with models without a peninsula and the topographic effect of the peninsula located upstream of the separation point of the mean flow is shown to be relatively small. If a peninsula is located downstream (east) of the separation point of the mean flow, a large meander path has a tendency to appear in the case with a relatively large NBI of more than 20° by the topographic effect of the peninsula, which is different from the previous two cases without a peninsula and with a peninsula located upstream of the separation point of the mean flow. If NBI exceeds 30°, only large meander path is commonly formed in all the cases, and the topographic effect of the peninsula is weak. It is found that both topographic effects of NBI and the peninsula located downstream of the separation of the mean flow are important for path dynamics of a western boundary current.

1. Introduction

There have been various studies on the path dynamics of western boundary currents. If nonlinear effects are neglected, a western boundary current is strongest along the western boundary (Stommel 1948; Munk 1950). However, if nonlinear effects are included, strong current shifts downstream and an enhanced flow along the northwestern boundary is formed (Munk et al. 1950). In case of no friction, the strongest current is formed along the northern boundary (Fofonoff 1954). These features are also shown by numerical models with different parameters (e.g., Veronis 1966; Ierley 1987).

The Kuroshio, a western boundary current in the North Pacific, has a bimodal path characteristic between a small-amplitude meander (straight) path and a large-amplitude meander path (Taft 1972; Nitani 1975; Ishii et al. 1983). As such a stationary large meander path is not observed in other western boundary currents, dynamics of the large meander path of the Kuroshio has been studied by many investigators. Before 1985, the large meander of the Kuroshio was considered as a stationary Rossby wave in the zonal mean flow (e.g., White and McCreary 1976) and a large meander path is formed when the current velocity is relatively small. However, in later studies after 1985 (Yoon and Yasuda 1987; Sekine 1990; Akitomo et al. 1991), the large meander path has a tendency to appear when the current velocity is relatively large. The difference between the two groups is that, if a zonal northern coastal boundary is assumed, the results before 1985 are obtained, while when the northern boundary inclination from the zonal direction (NBI: θ in Fig. 1) is included in the model, results similar to those after 1985 are obtained. From this, it is suggested that the effect of NBI is an important factor on the dynamics of the western boundary current. Sekine (1988) examined the effect of the NBI and showed that a western boundary current along a zonal northern boundary is unstable and a meandering flow is formed. In contrast, if a NBI greater than 20° is assumed, the western boundary current is stable and a nonlarge meander path along the northern boundary is formed.

In addition to the effect of a NBI, topographic effects of a peninsula have also been studied (e.g., Yamagata and Umatani 1989; Akitomo et al. 1991; Zhang and Sekine 1995a,b). In particular, Yamagata and Umatani pointed out that local topographic effects such as a peninsula may trigger a big change in nearshore currents. It is thus suggested that the combined effects of a peninsula and a NBI should be examined. In the present study, topographic effects of a peninsula in the northern boundary is studied with special reference to its dependence on the orientation of the NBI. Here, we assume a peninsula with a triangular shape, and its influence on the western boundary current is examined. In the following, a description of the numerical model will be made in the next section. Results of the numerical model will be mentioned in section 3, in which two groups of models, with and without a peninsula, are considered. A summary and discussion will be presented in section 4.

2. Numerical model

A barotropic ocean with a constant depth of 1000 m is assumed (Fig. 1). We adopt a Cartesian coordinate system on a β plane with the x axis to the east and the y axis to the north. The vertically integrated vorticity equations for a rigid-lid approximation and hydrostatic balance are

$$\frac{\partial z}{\partial t} = -\frac{\partial uz}{\partial x} - \frac{\partial vz}{\partial y} - \beta v + A_h \nabla^2 z, \qquad (2.1)$$

where the volume transport function is related to the relative vorticity:

$$z = \frac{\partial v}{\partial x} - \frac{\partial u}{\partial y} = \frac{\partial}{\partial x}\left(\frac{1}{h}\frac{\partial \phi}{\partial x}\right) + \frac{\partial}{\partial y}\left(\frac{1}{h}\frac{\partial \phi}{\partial y}\right). \qquad (2.2)$$

All symbols used in the above equations are tabulated in Table 1. Nondimensionalizing Eq. (2.1), by $(x, y) = L(x^*, y^*)$, $t = (L/U)t^* = (1/\beta L)t^*$, where L is the width of the inflow and U is the representative inflow velocity, (2.1) becomes (dropping primes)

$$\frac{\partial z}{\partial t} = -\mathrm{Ro}\left(\frac{\partial uz}{\partial x} + \frac{\partial vz}{\partial y}\right) - v + (1/\mathrm{Re})\nabla^2 z, \qquad (2.3)$$

where the nondimensional Reynolds number is $\mathrm{Re} = UL/A_h$, and the Rossby number is $\mathrm{Ro} = U/\beta L^2$.

The system is driven by an in- and outflow of 55 Sv (Sv $\equiv 10^6$ m^3 s^{-1}) where the inflow is at the southern boundary and the outflow at the eastern boundary (Fig. 1). The 55 Sv flow is assumed on the basis of observational results: the mean geostrophic volume transport, referred to 1000 db, is 43 (±3) Sv (Minami et al. 1979), and that referred to 1500 db is

61 (±7) Sv south of Japan [Sekine et al. (1991; cf. Fig. 1 of Sekine and Kutsuwada (1984)]. Detailed observations along ASUKA line off Shikoku including the data by direct current measurements (Imawaki 1996, personal communication; cf. Fig. 13 of Kagimoto and Yamagata 1997) show that the volume transport of the Kuroshio is 63 (±13) Sv.

A sinusoidal horizontal velocity distribution of the in/outflow is assumed and only the northward component is given at the southern open boundary:

$$\phi = \begin{cases} \phi_0 - \phi_0 \cos(\pi x/L_i) & \text{for } 0 \leqq x \leqq L_i \quad (2.4) \\ 2\phi_0 & \text{for } L_i \leqq x, \quad (2.5) \end{cases}$$

where ϕ_0 is one-half of the total transport of the in/outflow and L_i (=187 km) is the width of the inflow (Fig. 1). A similar boundary condition is imposed at the eastern outflow boundary:

$$\phi = \begin{cases} 2\phi_0 \quad \text{for } 0 \leqq y \leqq 1020.5 \text{ km} & (2.6) \\ \phi_0 + \phi_0 \cos(\pi(y - 1020.5)/L_o) & \\ \quad \text{for } 1020.5 \text{ km} \leqq y \leqq 1177.5 \text{ km} & (2.7) \\ 0 \quad \text{for } 1177.5 \text{ km} \leqq y, & (2.8) \end{cases}$$

where L_o (=157 km) is the width of the outflow. The maximum inflow velocity U_0 and mean velocity ($2U_0/\pi$) are 92 cm s^{-1} and 58 cm s^{-1}, respectively. Dependence of the numerical solution on the intensity of in/outflow velocity has been studied by use of various models. This representative velocity is expected to yield a multi-steady-state numerical solution (e.g., Yoon and Yasuda 1987; Akitomo et al. 1991) in which both large meander path and nonlarge meander path are possibly formed.

Although a constant L_i is assumed in all models, as shown in the results, L_i does not directly control the width of the mean flow. As shown in the results of numerical models, the mean flow width adjustments as it runs along the western boundary. Viscous boundary conditions are imposed on the western and simplified coastal boundaries, while a slip boundary condition is imposed on the remaining open boundaries. In the numerical calculation, we adopt a rectangular grid with horizontal spacing of 18.7 km in the west–east direction and 15.7 km in the south–north direction.

Because velocity U and width L of the Kuroshio in (2.3) have relatively small variation in comparison with that of the horizontal eddy viscosity A_h, with a range of two orders (10^6–10^8 cm^2 s^{-1}) at most, the parameters U, L, and $\beta = 2 \times 10^{-13}$ cm^{-1} s^{-1} are fixed and only A_h is changed (Table 2). In the present study, 24 cases of numerical models with different characteristics are examined. In the first step, a relatively small eddy viscosity with $A_h = 5 \times 10^8$ cm^2 s^{-1} is assumed and the effect of a northern boundary without a peninsula is examined by use of four models with different NBI (θ in Fig. 1). These models with a NBI angle of 0°, 10°, 20°, and 30° are referred to as NP00SE, NP10SE, NP20SE, and NP30SE, respectively (Table 2). In the next section, four similar experiments are performed assuming relatively large eddy viscosity $A_h = 1 \times 10^7$ cm^2 s^{-1} (NP00LE, NP10LE, NP20LE, and NP30LE).

In the second step, a peninsula is placed in the northern boundary, and its topographic effect is examined. Initially, a peninsula is placed upstream (west) of the separation point of the mean flow out from northernmost area in the western boundary region (Fig. 1b). Here, the separation point of the mean flow is estimated from the results of no peninsula performed in the first step. Assuming small eddy viscosity ($A_h = 5 \times 10^6$ cm^2 s^{-1}), four similar cases with different NBIs are examined (PC00SE, PC10SE, PC20SE, and PC30SE). Second, the peninsula is placed downstream (east) of the separation point and four models with different NBI are examined (PF00SE, PF10SE, PF20SE, and PF30SE).

Last, because of the results obtained in the models with the peninsula downstream of the separation point and in order to see the influence of the outflow condition, eight models with an eastward expanded domain are performed: the former four models with the larger horizontal eddy viscosity ($A_h = 1 \times 10^7$ cm^2 s^{-1}) and four different NBIs are referred to as LDPF00LE, LDPF10LE, LDPF20LE, and LDPF30LE, while the other four models with the small horizontal eddy viscosity ($A_h = 5 \times 10^6$ cm^2 s^{-1}) are referred to as LDPF00SE, LDPF10SE, LDPF20LE, and LDPF30SE. The the zonal distance of

the previous models shown in Fig. 1 is 1851.3 km, but that of the expanded models is 2318.8 km.

3. Results

a. Cases with no peninsula

Temporal variation of streamfunctions in the case with no peninsula and a zonal northern boundary (NP00SE and NP00LE) is shown in Fig. 2. In the former cases with relatively small eddy viscosity (NP00SE), a cyclonic eddy forms in the northwestern area and the mean flow shows a large meander path. The cyclonic eddy weakens after 45 days and stretches southward. Later, this cyclonic eddy is cut off from the mean flow and decay by day 55, while a new cyclonic eddy is generated in the eastern area and shifts westward.

The flow pattern at day 90 is similar to that on day 40 and decay of the new cyclonic eddy through a similar cutoff process is carried out in 120–125 days. In later time, similar spinup and spindown of the cyclonic eddy are repeated. In order to see these processes more clearly, temporal and spatial change in the volume transport of the cyclonic eddy are shown in Fig. 3a. The mean period of spinup and spindown of the cyclonic eddy is 70 days. Enhancement of volume transport of the cyclonic eddy is detected during the period of westward shift before cutoff from the mean flow. Cutoff of the cyclonic eddy is associated with the southward extension of the cyclonic eddy. Because eastward mean flow is weak around the southward expanded eddy, the southward expanded area of the cyclonic eddy shifts westward as a Rossby wave, which results in the cutoff of the cyclonic eddy from the eastward mean flow. If we consider variation in relative vorticity of the spindown and cutoff of the cyclonic eddy, its basic dynamics is almost similar to that in Yamagata and Umatani (1989).

The spinup and spindown of the cyclonic eddy with a period of 50 days occurs in NP00LE with relatively large eddy viscosity ($A_h = 10^7$ cm^2 s^{-1}) (Figs. 2b and 3b). The period of the cyclonic eddy of 50 days is shorter than that of NP00SE (70 days). It is shown from Fig. 3 that the maximum volume transport of the cyclonic eddy of NP00SE exceeds 50 Sv, while that of NP00LE is less than 40 Sv. The shorter period of the cyclonic eddy in NP00LE is caused by weak spinup and strong spindown of the cyclonic eddy due to the effect of large eddy viscosity.

Results of NP10SE shown in Figs. 4a and 3a are characterized by a long period of spinup and spindown of the cyclonic eddy (about 135 days) in comparison with NP00SE (70 days) in the initial stage. The longer period of NP10SE is mainly due to the small westward velocity of the cyclonic eddy shown in Fig. 3a by the enhanced eastward velocity of the mean flow as indicated by the smaller width of the concentrated volume transport function along the northern boundary (Fig. 4a). It should be noted that a change of the flow pattern occurs after 560 days (Figs. 3a and 5a). After cutoff of the cyclonic eddy on day 570, the remaining small cyclonic circulation on the coastal side of the mean flow is advected downstream by the mean flow along the coastal boundary. So spinup of the cyclonic eddy does not occur after the day 600 and only a nonlarge meander path with horizontally large anticyclonic circulation exists afterward.

As for the case NP10LE (Fig. 4b), a large meander path with spinup and spindown of the cyclonic eddy is maintained. The different result between NP10SE and NP10LE is a formation of the large anticyclonic circulation south of the mean flow in NP10SE, which enhances the current path along the northern boundary. This effect acts to trap the current path along the northern boundary and suppresses of formation of a large meander path. In contrast to this, such an anticyclonic eddy is not formed in NP10LE and the basic large meander path with spinup and spindown of the cyclonic eddy is maintained. Furthermore, it is suggested that formation of the large anticyclonic circulation south of the mean flow in NP10SE is due to the increase in nonlinearity by the small horizontal eddy viscosity, which relatively induces the northward intensified western boundary current with a large anticyclonic eddy represented by a Fofonoff solution rather than the westward intensified flow shown in a linear model such as a Munk solution (e.g., Veronis 1966; Ierley 1987). It is thus indicated that the nonlinear effect on the western boundary current, which enhances the coastal flow along northern boundary, has a tendency to suppress formation of a large meander path.

If NBI exceeds 20°, a nonlarge (small amplitude) meander path along the northern boundary is commonly formed. In case of NP20SE (Fig. 5b), a weak spinup of the cyclonic eddy occurs in the initial stage (Fig. 3a); however, the cyclonic eddy shifts eastward by advection of the mean flow. In a stationary state, a nonlarge meander path along the northern boundary with a weak separation in the outflow area is formed (Figs. 3a and 5b). The eastward shift of the cyclonic eddy and its combination with the cyclonic circulation in the outflow area are also carried out in NP20LE (Fig. 5c). However, the cyclonic circulation in the outflow area is weak and its southward shift does not occur in this case and a small amplitude meander path without separation is formed in a stationary state. As for NP30SE, although the cyclonic circulation in the outflow area is much enhanced, mean flow separation from the northern boundary is less than that of NP20SE. This is due to nonoccurrence of the southward development of the cyclonic circulation in the outflow area, which does occur in NP20SE. In contrast to this, the cyclonic circulation in the outflow area is very weak in NP30LE (Fig. 5e) and a nonlarge meander path along the northern boundary is formed. It is thus a result that although a flow pattern near the eastward outflow area is weakly different, a nonlarge meander path path along the northern boundary is commonly formed,

if the NBI exceeds 20°.

b. Cases with a peninsula

Results of models with a peninsula located upstream (west) of the separation point of the mean flow from the northernmost area in the western boundary region are shown in Fig. 6. As for the case of the zonal northern boundary (PC00SE), a large meander path with spinup and spindown of the cyclonic eddy at different time periods occurs east of the peninsula (Fig. 7a). Two dominant cyclonic eddies develop just downstream of the peninsula and farther into the eastern area. The former cyclonic eddy is formed by the topographic effect of the peninsula and the latter eddy is due to a Rossby lee wave. It is seen from Figs. 3a and 7a that the volume transport of the cyclonic eddy of PC00SE is less than that of NP00SE and spinup of the cyclonic eddy is relatively weak. This is due to the current path being just south of the peninsula, which suppresses free motion of a large meander path with spinup and spindown of the cyclonic eddy.

A nonlarge meander path along the northern boundary is formed in PC10SE (Fig. 6b). By suppressing the effect on spinup of the cyclonic eddy, which occurs in PC00SE, spinup and spindown of the cyclonic eddy are inhibited. After 100 days, weak separation of the mean flow is formed by the southward development of a cyclonic circulation in the outflow area (Fig. 7a). As for PC20SE, decay of the cyclonic circulation in the outflow area occurs by day 330 (Fig. 6c). After decay of the cyclonic circulation, southward development of the cyclonic circulation occurs and a separated mean flow is formed (Fig. 7a). Occurrence of the instability of the cyclonic circulation in the outflow area and the separated flow pattern of PC20SE is common to those of NP20SE shown in Fig. 5b. A nonlarge meander path along the northern boundary of PC30SE (Figs. 6d and 7a) is also common to NP30SE. Thus it results that the topographic effect of a peninsula located west of the separation point of the mean flow is weak in the case with large NBI. Although the topographic effect of the peninsula is relatively large for a small NBI, especially in PC00SE, total path patterns with the large meander path and the nonlarge meander path are not changed from those of no peninsula (Figs. 3 and 7a).

Results of the numerical model with a peninsula downstream (east) of the separation point of the mean flow out from northernmost area in the western boundary region are shown in Fig. 8. A large meander path with spinup and spindown of the cyclonic eddy with a period of 50 days is formed in PF00SE (Fig. 8a), for which the time period is shorter than NP00SE (70 days) and almost the same as in NP00LE (50 days). The shorter time period of the cyclonic eddy (Fig. 7b) is due to the smaller horizontal scale west of the peninsula, which results in a short time for the westward shift of the cyclonic eddy. As for PF10SE (Fig. 8b), after one cycle of spinup and spindown of the cyclonic eddy during the initial 80 days, a stationary weak meander path without spinup and spindown of the cyclonic eddy forms (Fig. 7b). This stationary weak meander path is mainly due to a northward intensification by the nonlinear effect, which is also detected in the formation of the anticyclonic circulation for the NP10SE case (Fig. 5a). It is also suggested that the stationary weak meander path is influenced by the cyclonic circulation formed in the outflow area north of the mean flow. The mean flow is forced to shift southward by the existence of this cyclonic circulation, and the mean flow separates from the northern boundary in the downstream region of the peninsula. This acts to decrease the topographic effect of the peninsula, and generation of the cyclonic eddy, which enhances the meander path, is weakened in this case.

As for PF20SE (Figs. 7b and 8c), a cyclonic eddy is gradually formed west of the peninsula by day 390. Cutoff of the cyclonic eddy occurs at day 460 and a new cyclonic eddy develops by day 480. At the later time, a large meander path with spinup and spindown of the cyclonic eddy west of the peninsula is maintained. As the mean flow has a greater tendency to flow along the northern boundary and the topographic effect of the peninsula is enhanced, the occurrence of the spinup and spindown of the cyclonic eddy is enhanced. As for PF30SE (Fig. 8d), a nonlarge meander path along the northern boundary is formed by the effect of a large NBI. This result is common to all of the previous cases without the peninsula (Figs. 5d,e) and with the peninsula located in the upstream region (Fig. 6d). In general, the result is that the range of the large meander path is expanded to NBI of 20° in the case of a peninsula located downstream region of the separation point of the mean flow.

Results of the eastward expanded models are shown by temporal and spatial changes of the intensity of the cyclonic eddy in Fig. 9. In comparison with Fig. 7b, an almost similar flow pattern to PF00SE with a longer period of spinup and spindown of the cyclonic eddy is found in LDPF00SE. A similar flow pattern difference between NP00SE and NP00LE, shown in Fig. 3, is detected between LDPF00SE and LDPF00LE. The volume transport of the cyclonic eddy of LDPF00SE is less than that of PF00LE. Because confinement of the main current path to the northern boundary is weak in LDPF00LE, the topographic effect of the peninsula is also weakened by less probability for the current path to approach to the peninsula. Furthermore, since the volume transport of the cyclonic eddy is significantly decreased in LDPF00LE (Fig. 9b), the topographic effect of the peninsula is much influenced by the horizontal eddy viscosity. On the other hand, it is noticed that the lifetime of the cyclonic eddy of LDPF00SE and LDPF00LE (Fig. 9a) is longer than that of PF00SE (Fig. 7b), which is due to the less confinement of the main current path to the northern boundary that gives large spindown effect.

Although the weak meander path without spinup and spindown of the cyclonic eddy is formed in a stationary state of

PF10SE (Fig. 7b), a large meander path with spinup and spindown of the cyclonic eddy is maintained stationary in LDPF10SE and LDPF10LE (Fig. 10). The total flow patterns of the eastward expanded models relatively resemble those of no peninsula shown in Fig. 3, except for the formation of the cyclonic circulation east of the peninsula. Namely, the large meander path is maintained for a longer period in NP10SE and a large, stationary meander path is formed in NP10LE; however, the weak meander paths without spinup and spindown of the cyclonic eddy are formed in NP10SE (Fig. 5a), PC10SE (Fig. 6b), and PF10SE (Fig. 8b). It is shown from Fig. 10 that the current path in the downstream region of the peninsula has a relatively free motion with the formation of the cyclonic eddy east of the peninsula, which is quite different from the stationary weak meander formed in NP10SE, PC10SE, and PF10SE. Because the effect of the northward shift of the western boundary current by the nonlinear effect denoted above is common to these models, it thus results that the weak meander paths without the spinup and spindown of the cyclonic eddy formed in PF10SE, PC10SE, and NP10SE are caused by the cyclonic circulation in the outflow area.

The total flow patterns of LDPF20SE and LDPF20LE resemble that of PF20SE (Fig. 7b), while only a nonlarge meander path is formed in NF20SE and NP20LE (Fig. 3). Here, to see further temporal variation in LDPF20SE, time integration is carried out (Fig. 11). In a stationary state, a large meander path with spinup and spindown of the cyclonic eddy is maintained, similar to PF20SE (Fig. 7b). The result is that the NBI range of the large meander path is expanded to more than 20° by the topographic effect of the peninsula located downstream of the separation point of the mean flow. In the case of NBI = 30°, a nonlarge meander path along the northern boundary is formed in LDPF30SE and LDPF30LE, which is common to all the previous cases. A critical NBI less than 30° exists over which the effects of the peninsula are very weak and only a nonlarge meander path along the northern boundary is formed.

4. Summary and discussion

Dynamics of the western boundary current flowing along a northern boundary with and without a peninsula have been examined with special reference to the degree of northern boundary inclination from a zonal direction (NBI: θ in Fig. 1) and the location of the peninsula. The main results of the numerical experiments are summarized as follows.

1. If a peninsula is located upstream (west) of the separation point of the mean flow out from the northernmost area in the western boundary region, a large meander path with irregular oscillations is formed in the case of no NBI (PC00SE). A straight path with a small cyclonic circulation just downstream of the peninsula is formed in cases of NBIs larger than 10° (PC10SE, PC20SE, and PC30SE).

2. Overall, flow patterns in the cases with the peninsula upstream (west) of the separation point of the mean flow are quite similar to those without a peninsula. A large meander path is formed in the case with small NBI. A minor difference is that spinup and spindown of the cyclonic eddy in the case of no peninsula with a zonal northern boundary (NP00SE) is changed to be an irregular oscillation of the mean flow (PC00SE), and the small cyclonic eddy is formed just downstream of the peninsula.

3. If a peninsula is located downstream (east) of the separation point of the mean flow from the northernmost area in the western boundary region, the range with the large meander path with spinup and spindown of the cyclonic eddy is expanded to large NBI more than 20°, while it is confined to small NBI less than 10° in cases of no peninsula and of the peninsula located upstream of the separation point of the mean flow. The expansion of the large meander path is due to the formation of cyclonic eddy by the topographic effect of peninsula.

In general, both topographic effects of a NBI and a peninsula east (downstream) of the separation point of the mean flow are shown to be important for the path dynamics of the western boundary current. We discuss the difference in the main flow pattern between the Florida Current with a straight coastal flow and the Kuroshio with a bimodal path between a large meander path and nonlarge meander path. The representative NBI of the Florida Current is about 45°, while that of the Kuroshio is about 20°. Because the NBI of the Florida Current is greater than 30° and because no peninsula exists on a scale similar to that of the present study (the Florida Strait is too large to change the mean flow pattern discussed above), it is suggested that the Florida Current is more likely to follow a straight path. In contrast, some peninsulas on a scale similar to the present model exist in the Kuroshio region south of Japan. Together with an NBI of about 20°, it is suggested that the Kuroshio has a tendency to take a large meander path.

The weak meander path without spinup and spindown of the cyclonic eddy is formed in PF10SE due to the effect of enhanced cyclonic circulation in the outflow region, while a large meander path with spinup and spindown of the cyclonic eddy is formed in LDPF10SE and LDPF10LE with an eastward expanded domain (Figs. 9 and 10). These results suggests that, if the outflow is fixed in southern (offshore) latitudes such as in PF10SE, the topograpbic effect of the peninsula is decreased and a nonlarge meander path forms. However, these conditions are rarely established in the actual ocean; the results of LDPF10SE and LDPF10LE are more general in comparison with those of PF10SE.

The actual range of the large meander path and nonlarge meander path of the Kuroshio south of Japan is also influenced

by the intensity of the mean flow (e.g., Yoon and Yasuda 1986; Yamagata and Umatani 1989; Sekine 1990; Akitomo et al. 1991), in which there exist three ranges with only large meander path, multisteady state between large meander path and nonlarge meander path, and only nonlarge meander path. Although the NBI and the shape of the peninsula are fixed for the case of the Kuroshio south of Japan, they can be considered as variables, because the direction of the mean flow is changed depending on its path pattern, then the NBI relative to the mean flow and the actual topographic effect of the peninsula are changed depending on the flow pattern of the mean current. It is pointed out that the distribution of the ranges of the large meander path and nonlarge meander path is not specified by only the intensity of the mean flow, and the topographic effects of NBI and peninsulas should be also included for the dynamics of path selection of the Kuroshio. It is noticed that there exist some peninsulas, such as the Kyushu, Muroto-Misaki, and Kii Peninsula on the southern coast of Japan. Therefore, detailed topographic effects of these peninsulas and their interactions should be examined in the next stage of this study. The topographic effects of two peninsulas will be studied in the succeeding study with reference to the dependence on NBI.

Acknowledgments

I would like to thank two anonymous reviewers for their valuable comments that helped to clarify this manuscript. The numerical calculations were carried out on a VP-2600 of Nagoya University and on a FACOM M-760 of Mie University. The author would also like to thank Mr. A. Aso for his help in numerical calculation. This study was supported by a Grand in Aid for Scientific Research from the Ministry of Education, Science of Culture of Japan (05640475).

REFERENCES

Akitomo, K., T. Awaji, and N. Imasato, 1991: Kuroshio path variation south of Japan. 1: Barotropic inflow-outflow model. *J. Geophys. Res.,* **96,** 2549–2560..

Fofonoff, N. P., 1954: Steady flow in a frictionless homogeneous ocean. *J. Mar. Res.,* **13,** 254–262..

Ierley, G. R., 1987: On the onset of recirculation in barotropic general circulation models. *J. Phys. Oceanogr.,* **17,** 2366–2374.. Find this article online

Ishii, H., Y. Sekine, and Y. Toba, 1983: Hydrographic structure of the Kuroshio large cold water mess region down to the deeper layers of the ocean. *J. Oceanogr. Soc. Japan,* **39,** 240–250..

Kagimoto, T., and T. Yamagata 1997: Seasonal transport variations of the Kuroshio: An OGCM simulation. *J. Phys. Oceanogr.,* **27,** 403–418.. Find this article online

Minami, H., E. Kamihira, K. Komuma, H. Eguchi, and J. Nishizawa, 1979: Statistical features of the oceanic conditions south of Honshu, Japan. Part 2: In spring and autumn off Kii Peninsula (in Japanese with English abstract). *Bull. Kobe Mar. Obs.,* **197,** 1–11..

Moore, D. W., 1963: Rossby waves in ocean circulation. *Deep-Sea Res.,* **10,** 735–747..

Munk, W. H., 1950: On the wind-driven ocean circulation. *J. Meteor.,* **7,** 79–93..

— ,G. W. Groves, and G. F. Carrier, 1950: Note on the dynamics of the Gulf Stream. *J. Mar. Res.,* **9,** 218–238..

Nitani, H., 1975: Variation of the Kuroshio south of Japan. *J. Oceanogr. Soc. Japan,* **31,** 154–173..

Sekine, Y., 1988: Coastal and bottom topographic effects on the path dynamics of the western boundary current with special reference to the Kuroshio south of Japan. *La mer,* **26,** 99–144..

— ,1990: A numerical experiment on the path dynamics of the Kuroshio with reference to the formation of the large meander path south of Japan. *Deep-Sea Res.,* **37,** 359–380..

— ,and K. Kutsuwada, 1994: Seasonal variation in volume transport of the Kuroshio south of Japan. *J. Phys. Oceanogr.,* **24,** 261–272.. Find this article online

— ,Y. Sato, H. Takamori, and I. Sakamoto, 1991: Observation on the volume transport of the Kuroshio south of Japan. *Bull. Mie Univ.,* **6,** 57–82..

Stommel, H., 1948: The westward intensification of wind-driven ocean currents. *Trans. Amer. Geophys. Union,* **29,** 202–206..

Taft, B. A., 1972: Characteristics of the flow of the Kuroshio south of Japan. *Kuroshio—Its Physical Aspects,* H. Stommel and K. Yoshida, Eds., University of Tokyo Press, 165–214..

Veronis, G., 1966: Wind-driven ocean circulation, Part II. *Deep-Sea Res.*, **13,** 30–35..

White, W. B., and J. P. McCreary, 1976: The Kuroshio meander and its relationship to the large scale ocean circulation. *Deep-Sea Res.*, **23,** 33–47..

Yamagata, T., and S. Umatani, 1989: Geometory-forced coherent structure as a model of the Kuroshio large meander. *J. Phys. Oceanogr.*, **19,** 130–138.. Find this article online

Yoon, J. H., and I. Yasuda, 1987: Dynamics of the Kuroshio large meander. Two-layer model. *J. Phys. Oceanogr.*, **17,** 66–81.. Find this article online

Zhang, M., and Y. Sekine, 1995a: A numerical experiment on the path dynamics of the Kuroshio south of Japan. Part I. Coastal topographic effect. *La mer*, **33,** 63–75..

— , and — , 1995b: A numerical experiment on the path dynamics of the Kuroshio south of Japan. Part I: Bottom topographic effect. *La Mer*, **33,** 77–87..

Tables

Table 1. Lists of symbols.

t	Time
x	Eastward component of Cartesian coordinate
y	Northward component of Cartesian coordinate
u	x-directed (eastward) component of velocity
v	y-directed (northward) component of velocity
h	Depth of ocean
z	Relative vorticity
ϕ	Volume transport function
β	Linear change rate of the Coriolis parameter
A_h	Coefficient of horizontal eddy viscosity
∇^2	Laplacian operator for the horizontal direction

Click on thumbnail for full-sized image.

Table 2. Parameters of the numerical models.

Run	NBI ($\theta°$)	Peninsula (location)* (km)	A_h (10^6 cm^2 s^{-1})	Zonal length of the model (km)
NP00SE	0	No	5	1851.3
NP10SE	10	No	5	1851.3
NP20SE	20	No	5	1851.3
NP30SE	30	No	5	1851.3
NP00LE	0	No	10	1851.3
NP10LE	10	No	10	1851.3
NP20LE	20	No	10	1851.3
NP30LE	30	No	10	1851.3
PC00SE	0	Yes (168.3)	5	1851.3
PC10SE	10	Yes (168.3)	5	1851.3
PC20SE	20	Yes (168.3)	5	1851.3
PC30SE	30	Yes (168.3)	5	1851.3
PF00SE	0	Yes (785.4)	5	1851.3
PF10SE	10	Yes (785.4)	5	1851.3
PF20SE	20	Yes (785.4)	5	1851.3
PF30SE	30	Yes (785.4)	5	1851.3
LDPF00SE	0	Yes (785.4)	5	2318.8
LDPF10SE	10	Yes (785.4)	5	2318.8
LDPF20SE	20	Yes (785.4)	5	2318.8
LDPF30SE	30	Yes (785.4)	5	2318.8
LDPF00LE	0	Yes (785.4)	10	2318.8
LDPF10LE	10	Yes (785.4)	10	2318.8
LDPF20LE	20	Yes (785.4)	10	2318.8
LDPF30LE	30	Yes (785.4)	10	2318.8

*"d" in Fig. 1.

Click on thumbnail for full-sized image.

Figures

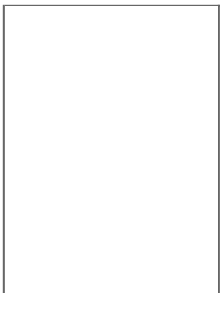

Click on thumbnail for full-sized image.

Fig. 1. Schematic view of the model ocean shown by stippled area. (a) Four cases with different northern coastal boundary inclination (NBI) from the zonal direction. (b) As in (a) but for either of two peninsulas. The hatched areas with closed arrows in (a) indicate the boundary with in/outflow.

Click on thumbnail for full-sized image.

Fig. 2. Results of the numerical model without a peninsula, shown by isopleths of volume transport function for (a) NP00SE and (b) NP00LE. The contour interval of the transport function is 20 Sv and areas with negative volume transport function are stippled. Integrated time from the initial state (0 days) is shown in upper left of each panel.

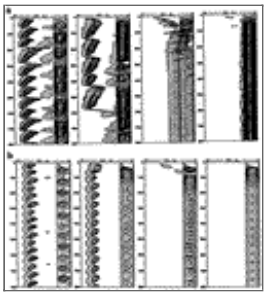

Click on thumbnail for full-sized image.

Fig. 3. Temporal and spatial change of the intensity of a cyclonic eddy in the cases without a peninsula shown in Fig. 1a. (a) Cases with small eddy viscosity ($A_h = 5 \times 10^6$ cm^2 s^{-1}). From left to right, NBI is 0° (NP00SE), 10° (NP10SE), 20° (NP20SE), and 30° (NP30SE). (b) Cases with large eddy viscosity ($A_h = 1 \times 10^7$ cm^2 s^{-1}). From left to right, NBI is 0° (NP00LE), 10° (NP10LE), 20° (NP20LE), and 30° (NP30LE). The intensity of the cyclonic eddy is defined by the minimum value of the volume transport function along the south–north direction. Contour interval is 10 Sv and regions with negative volume transport function are stippled.

Click on thumbnail for full-sized image.

Fig. 4. As in Fig. 2 but for the cases with NBI 10°: (a) NP10SE and (b) NP10LE.

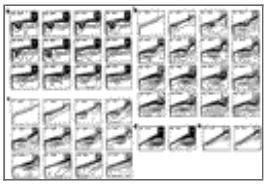

Click on thumbnail for full-sized image.

Fig. 5. As in Fig. 2 but for the cases with different NBI: (a) NP10SE, (b) NP20SE, (c) NP20LE, (d) NP30SE, and (e) NP30LE.

Click on thumbnail for full-sized image.

Fig. 6. Results of the numerical model with a peninsula west of the separation of the mean flow from the northernmost area in the western boundary region: (a) PC00SE, (b) PC10SE, (c) PC20SE, and (d) PC30SE.

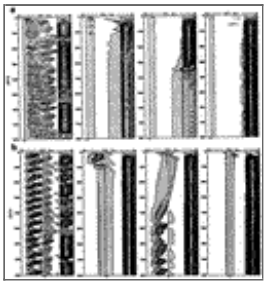

Click on thumbnail for full-sized image.

Fig. 7. As in Fig. 3 but for the cases with a peninsula. (a) Cases with a peninsula west of the separation point of the mean flow. From left to right, NBI is 0° (PC00SE), 10° (PC10SE), 20° (PC20SE), and 30° (PC30SE). (b) Cases with a peninsula east of the separation point of the mean flow. From left to right, NBI is 0° (PF00SE), 10° (PF10SE), 20° (PF20SE), and 30° (PF30SE). Location of the peninsula is shown by a triangle with two vertical bars in the bottom of each panel.

Click on thumbnail for full-sized image.

Fig. 8. As in Fig. 6 but for the case with a peninsula east of the separation point of the mean flow: (a) PF00SE, (b) PF10SE, (c) PF20SE, and (d) PF30SE.

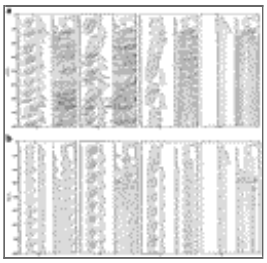

Click on thumbnail for full-sized image.

Fig. 9. As in Fig. 3 but for the cases with an eastward expanded area. (a) Cases with small eddy viscosity; (b) cases with large eddy viscosity. The contour interval is 10 Sv.

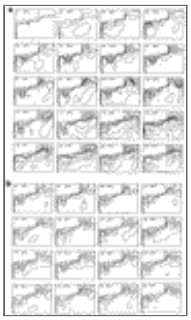

Click on thumbnail for full-sized image.

Fig. 10. Numerical results with the eastward expanded area shown by isopleths of the volume transport function: (a) LDPF10SE, (b) LDPF10LE. The contour interval of the transport function is 20 Sv and areas with negative volume transport function are stippled.

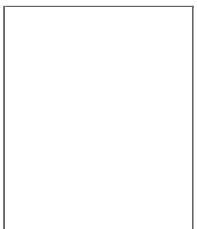

Click on thumbnail for full-sized image.

Fig. 11. Temporal and spatial changes of the intensity of cyclonic eddy in LDPF20SE during 800–1600 days. Contour interval is 10 Sv.

Corresponding author address: Dr. Yoshihiko Sekine, Institute of Oceanography, Faculty of Bioresource, Mie University, 1515 Kamihama, Tsu, Mie 512, Japan.

E-mail: sekine@bio.mie-u.ac.jp

top